Journal of Solid State Chemistry **142,** 180–186 (1999)
Article ID jssc.1998.8021, available online at http://www.idealibrary.com on IDEAL®

Structure and Properties of $Nd_5Ni_6In_{11}$

Rainer Pöttgen,*,[1] Rolf-Dieter Hoffmann,* Reinhard K. Kremer,† and Walter Schnelle†

*Anorganisch-Chemisches Institut, Universität Münster, Wilhelm-Klemm-Strasse 8, D-48149 Münster, Germany; and
†Max-Planck-Institut für Festkörperforschung, Heisenbergstrasse 1, D-70569 Stuttgart, Germany

Received May 11, 1998; in revised form August 24, 1998; accepted September 7, 1998

The title compound was prepared from the elements by a reaction in an arc melting furnace and subsequent annealing at 970 K. $Nd_5Ni_6In_{11}$ crystallizes with the orthorhombic $Pr_5Ni_6In_{11}$-type structure: *Cmmm*, $a = 1455.9(3)$ pm, $b = 1453.3(3)$ pm, $c = 438.3(1)$ pm, $V = 0.9274(2)$ nm^3, $wR_2 = 0.0551$, 1086 F^2 values, and 42 variables. The structure of $Nd_5Ni_6In_{11}$ is built up from a complex three-dimensionally infinite $[Ni_6In_{11}]$ polyanionic network in which the neodymium atoms occupy pentagonal and hexagonal channels. Magnetic susceptibility measurements indicate Curie–Weiss behavior above 150 K with an experimental magnetic moment of 3.60(5) μ_B/Nd and a paramagnetic Curie temperature of −18(1) K. Antiferromagnetic ordering is detected at $T_N = 11.4(1)$ K. Field- and temperature-dependent magnetization data indicate a complex magnetic phase diagram with spin reorientations into three antiferro- and one ferrimagnetic phase. The magnetic data are supported by specific heat measurements. $Nd_5Ni_6In_{11}$ is a metallic conductor with a specific resistivity of 120 μΩ cm at room temperature. © 1999 Academic Press

Key Words: **$Nd_5Ni_6In_{11}$; antiferromagnetism; metallic behavior; specific heat.**

INTRODUCTION

The ternary systems rare earth metal–nickel–indium have intensively been investigated in the past. Several new compounds within these systems have been examined by X-ray diffraction on single crystals and powders (1); however, physical properties have been reported only for a few of these compounds (2).

Some years ago, Kalychak *et al.* (3) reported on the synthesis of the ternary intermetallics $R_5Ni_6In_{11}$ (R = La, Ce, Pr) and they determined the crystal structure of the praseodymium compound. More recently, Tang *et al.* (4) investigated the low-temperature properties of $La_5Ni_6In_{11}$ and $Ce_5Ni_6In_{11}$. The latter compound has a large electronic specific heat coefficient γ of 145 mJ/mol Ce atom K^2, indicating that $Ce_5Ni_6In_{11}$ is an intermediate heavy fermion system.

In the course of our studies on ternary indium intermetallics (5–12), we synthesized the isotypic compound $Nd_5Ni_6In_{11}$. Herein we report the structure refinement from X-ray single-crystal data as well as detailed magnetic susceptibility, electrical resistivity, and specific heat measurements of $Nd_5Ni_6In_{11}$. The existence of $Nd_5Ni_6In_{11}$ was recently indicated by Kalychak (13); however, no crystallographic data were reported.

EXPERIMENTAL

Starting materials for the preparation of $Nd_5Ni_6In_{11}$ were ingots of neodymium (Johnson Matthey), nickel wire (Johnson Matthey, ∅ 0.38 mm), and indium tear drops (Johnson Matthey), all with stated purities better than 99.9%. The large neodymium ingots were cut into small pieces in a drybox and kept under argon prior to the reactions. In a first step, small pieces of neodymium were melted to buttons in an arc furnace under an argon pressure of about 800 mbar. The argon was purified over molecular sieves, titanium sponge (900 K), and an oxisorb catalyst (14). The neodymium button was then melted together with the nickel wire and the indium droplets in the ideal 5:6:11 atomic ratio. The melted ingot was turned over and remelted three times on each side to ensure homogeneity, and it was subsequently annealed in an evacuated sealed silica tube at 970 K for 2 weeks.

The purity of the sample was checked by a Guinier powder pattern using Cu$K\alpha_1$ radiation and α-quartz (a = 491.30 pm, c = 540.46 pm) as an internal standard. The lattice constants (Table 1) were obtained by a least-squares refinement of the powder data. The indexing of the diffraction lines was facilitated by intensity calculations (15) using the positional parameters of the refined structure.

Single-crystal intensity data were collected by use of a four-circle diffractometer (Enraf-Nonius CAD4) with graphite-monochromatized Ag$K\alpha$ radiation and a scintillation counter with pulse height discrimination. All relevant data concerning the data collection are listed in Table 1.

The magnetic susceptibilities of polycrystalline pieces were determined with VTS (S.H.E. Inc.) and MPMS

[1] To whom correspondence should be addressed.

0022-4596/99 $30.00

TABLE 1
Crystal Data and Structure Refinement for $Nd_5Ni_6In_{11}$

Empirical formula	$Nd_5Ni_6In_{11}$
Formula weight	2336.48 g/mol
Temperature	293(2) K
Wavelength	56.086 pm
Crystal system	Orthorhombic
Space group	*Cmmm* (No. 65)
Unit cell dimensions	$a = 1455.9(3)$ pm
(Guinier powder data)	$b = 1453.3(3)$ pm
	$c = 438.3(1)$
	$V = 0.9274(2)$ nm^3
Formula units per cell	$Z = 2$
Calculated density	8.37 g/cm^3
Crystal size	$50 \times 50 \times 75$ μm^3
Data collection method	Enraf-Nonius, CAD4
Absorption correction	From ψ-scan data
Transmission ratio (max/min)	1.17
Absorption coefficient	17.4 mm^{-1}
$F(000)$	2014
θ range for data collection	2–26°
Scan type	ω–θ
Range in *hkl*	$0 \le h \le +22$, $0 \le k \le +22$, $-6 \le l \le 6$
Total number of reflections	1966
Independent reflections	1090 ($R_{int} = 0.0264$)
Reflections with $I > 2\sigma(I)$	982 ($R_\sigma = 0.0276$)
Refinement method	Full-matrix least-squares on F^2
Data/restraints/parameters	1086/0/42
Goodness-of-fit on F^2	1.257
Final R indices [$I > 2\sigma(I)$]	$R_1 = 0.0221$, $wR_2 = 0.0521$
R indices (all data)	$R_1 = 0.0268$, $wR_2 = 0.0551$
Extinction coefficient	0.0024(1)
Largest difference peak and hole	2434 and -2158 e/nm^3

(Quantum Design, Inc.) SQUID magnetometers between 2 and 300 K with magnetic flux densities up to 7 T.

The specific resistivities were measured on a small block ($0.9 \times 1.0 \times 1.1$ mm^3) with a conventional four-probe technique. Cooling and heating curves measured between 4.2 and 300 K were identical within the error bars.

The sample for the heat capacity measurement (112 mg) was mounted on the sapphire sample holder of the calorimeter. The addenda heat capacity was measured separately and subtracted. We used the quasiadiabatic step-heating method (Nernst's method) as described, e.g., in (16). The error in $c_p(T)$ between 2 and 20 K is $<2\%$.

RESULTS AND DISCUSSION

Powders and single crystals of $Nd_5Ni_6In_{11}$ are light gray and stable in air over long periods of time. No decomposition whatsoever was observed after several months. The needle-shaped single crystals exhibit metallic luster.

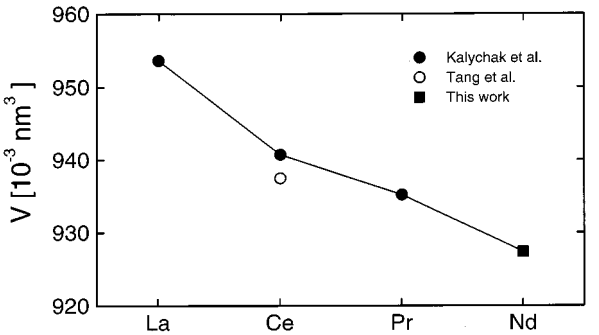

FIG. 1. Cell volumes of orthorhombic $Pr_5Ni_6In_{11}$-type compounds.

Lattice Constants

To date, four isotypic intermetallics with $Pr_5Ni_6In_{11}$-type structure are known, namely, $La_5Ni_6In_{11}$, $Ce_5Ni_6In_{11}$, $Pr_5Ni_6In_{11}$, and $Nd_5Ni_6In_{11}$. The lattice constants of these compounds decrease from the lanthanum to the neodymium compound as expected from the lanthanoid contraction. The plot of the cell volumes (Fig. 1), however, shows a deviation from a straight line, indicating partial tetravalent character of the cerium atoms in $Ce_5Ni_6In_{11}$. This is quite surprising, since the susceptibility data of Tang *et al.* (4) resulted in an experimental magnetic moment of $\mu_{exp} = 2.57(5)$ μ_B/Ce atom, close to the value of 2.54 μ_B for the free Ce^{3+} ion. We should further note that the cell volume of $Ce_5Ni_6In_{11}$ refined by Tang *et al.* (4) of 0.9375 nm^3 is even smaller than the cell volume of 0.9407 nm^3 given by Kalychak *et al.* (3) in the original work.

Structure Refinement

Single crystals of $Nd_5Ni_6In_{11}$ were isolated from the crushed samples after the annealing process and then examined by Buerger precession photographs to establish both symmetry and suitability for intensity data collection. The photographs (reciprocal layers *hk*0 and *h*0*l*) showed orthorhombic Laue symmetry *mmm* and the only systematic extinctions were those for a *C*-centered lattice. The structure refinement eventually showed that the space group with the highest symmetry compatible with these extinctions, *Cmmm*, was the correct one, in agreement with the previous results for the praseodymium compound (3). All relevant crystallographic data and experimental details are listed in Table 1.

The starting atomic positions were deduced from an automatic interpretation of direct methods with SHELX-86 (17) and the structure was successfully refined with SHELXL-93 (18) with anisotropic displacement parameters for all atoms. Within the refinement procedure, four reflections with $F_o^2 \le -2\sigma(F_o^2)$ were treated as unobserved (18). A final difference Fourier synthesis was flat and revealed no significant residual peaks. The results of the refinements are

TABLE 2
Atomic Coordinates and Anisotropic Displacement Parameters (pm^2) for $Nd_5Ni_6In_{11}$[a]

Atom	*Cmmm*	*x*	*y*	*z*	U_{11}	U_{22}	U_{33}	U_{12}	U_{eq}
Nd1	8*p*	0.36312(2)	0.32707(2)	0	90(1)	75(1)	82(2)	3(1)	82(1)
Nd2	2*c*	1/2	0	1/2	108(3)	77(3)	123(3)	0	102(1)
Ni1	8*p*	0.41631(6)	0.13776(6)	0	90(3)	109(4)	95(4)	−18(3)	98(2)
Ni2	4*j*	0	0.90603(8)	1/2	109(5)	78(5)	97(5)	0	94(2)
In1	8*q*	0.30711(3)	0.15654(3)	1/2	77(2)	96(2)	84(2)	−9(1)	86(1)
In2	4*g*	0.69593(4)	0	0	94(3)	78(2)	108(3)	0	93(1)
In3	4*h*	0.16074(4)	0	1/2	84(2)	79(2)	97(3)	0	87(1)
In4	4*j*	0	0.72474(4)	1/2	74(2)	74(2)	81(3)	0	76(1)
In5	2*a*	0	0	0	118(4)	69(3)	83(4)	0	90(2)

[a] U_{eq} is defined as one-third of the trace of the orthogonalized U_{ij} tensor. The anisotropic displacement factor exponent takes the form:

$$-2\pi^2[(ha^*)^2U_{11} + \ldots + 2hka^*b^*U_{12}].\ U_{13} = U_{23} = 0.$$

summarized in Table 1. Atomic coordinates and interatomic distances are listed in Tables 2 and 3. A projection of the crystal structure is presented in Fig. 2. Listings of the anisotropic displacement parameters and the observed and calculated structure factors are available.[2]

Crystal Chemistry

The present structure refinement of $Nd_5Ni_6In_{11}$ from single-crystal X-ray data confirms the previous structure determination by Kalychak *et al.* (3) for $Pr_5Ni_6In_{11}$; however, the present data are more precise. Comparing the atomic parameters of both refinements, we observed some inconsistencies. The *x* parameter of atom In2 and the *y* parameters of atoms Ni2 and In4 differed by a factor of 1/2 between the refinements, most likely indicating a printing error in Ref. (3), since these atomic coordinates furthermore did not match with the given projection of the structure.

Both neodymium positions in $Nd_5Ni_6In_{11}$ have high coordinations numbers (CN) as is typical for such intermetallic compounds. Nd1 has CN 15 with 3 Ni, 10 In, and 2 Nd atoms in the coordination shell, where Nd2 has the higher CN 18 with 8 Ni and 10 In atoms, respectively. There are no close Nd1–Nd2 interactions in the structure. The shortest interactions are Nd1–Nd1 at 398 and 399 pm, followed by Nd1–Nd1 and Nd2–Nd2 at 438 pm (lattice period *c*). These Nd–Nd distances are all significantly longer than the average Nd–Nd distance of 368 pm in elemental close-packed neodymium (19) with a stacking sequence ABAC. Thus, bonding Nd–Nd interactions can safely be neglected.

[2] Details may be obtained from Fachinformationszentrum Karlsruhe, D-76344 Eggenstein-Leopoldshafen, Germany, by quoting the registry number CSD-410093.

TABLE 3
Interatomic Distances (pm) in the Structure of $Nd_5Ni_6In_{11}$[a]

Nd1:	1	Ni1	285.8	In1:	2	Ni1	272.1
	2	Ni2	317.7		1	In4	297.8
	1	In5	320.7		1	In3	311.7
	2	In4	331.4		2	In2	315.9
	2	In1	331.7		1	In1	318.5
	2	In3	335.3		2	Nd1	331.7
	2	In1	340.7		2	Nd1	340.7
	1	In2	349.9		1	Nd2	361.4
	1	Nd1	398.4				
	1	Nd1	398.6	In2:	2	Ni1	258.4
	2	Nd1	438.3[b]		2	In3	302.6
					4	In1	315.9
Nd2:	8	Ni1	320.9		2	Nd1	349.9
	2	In4	326.6		2	Nd2	359.7
	4	In2	359.7				
	4	In1	361.4	In3:	2	Ni2	270.9
	2	Nd2	438.3[b]		2	In2	302.6
					2	In1	311.7
Ni1:	1	Ni1	243.7		2	In5	320.6
	1	In2	258.4		4	Nd1	335.3
	2	In1	272.1				
	2	In4	280.8	In4:	1	Ni2	263.5
	1	Nd1	285.8		4	Ni1	280.8
	2	Nd2	320.9		2	In1	297.8
					1	Nd2	326.6
Ni2:	2	In5	258.2		4	Nd1	331.4
	1	In4	263.5				
	2	In3	270.9	In5:	4	Ni2	258.2
	1	Ni2	273.1		4	In3	320.6
	4	Nd1	317.7		4	Nd1	320.7

[a] All distances shorter than 480 pm (Nd–Nd, Nd–In), 435 pm (Ni–In, In–In), and 400 pm (Nd–Ni, Ni–Ni) are listed. Standard deviations are all equal to or less than 0.2 pm.
[b] Not drawn in the coordination polyhedra of Fig. 3.

The coordination polyhedra are different for both neodymium atoms (Fig. 3). The Nd1 atoms are located in distorted pentagonal prismatic channels of the three-dimensional Ni–In network (Fig. 4), while the Nd2 atoms are situated in larger distorted hexagonal prismatic channels. The closest distance between the centers of the different channel types is 560 pm. Nd1 has the closer contacts to the neighboring nickel and indium atoms with average Nd–Ni and Nd–In distances of 307 and 335 pm, while these distances amout to 321 and 354 pm for Nd2. The larger distances for Nd2 certainly also reflect the higher coordination number. The most striking distance within these polyhedra, however, is the short Nd1–Ni contact at 286 pm. This by far shortest Nd-Ni distance in the structure of $Nd_5Ni_6In_{11}$ is only slightly larger than the sum of the metallic single-bond radii of 279 pm for Nd and Ni (20).

Both nickel positions in $Nd_5Ni_6In_{11}$ have different coordination spheres. Ni1 forms Ni–Ni dumbbells with a

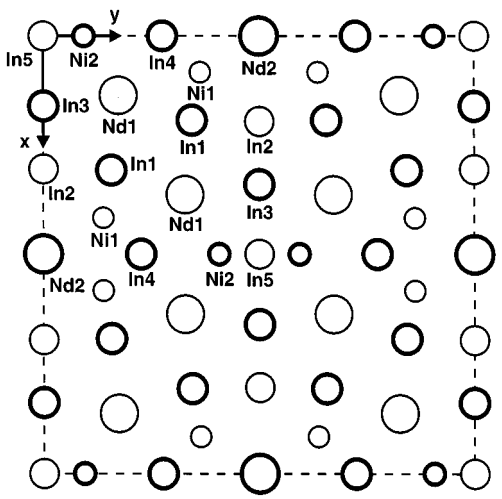

FIG. 2. Projection of the crystal structure of $Nd_5Ni_6In_{11}$ onto the xy plane. Atoms drawn by thin and thick lines are at $z = 0$ and $z = 1/2$, respectively.

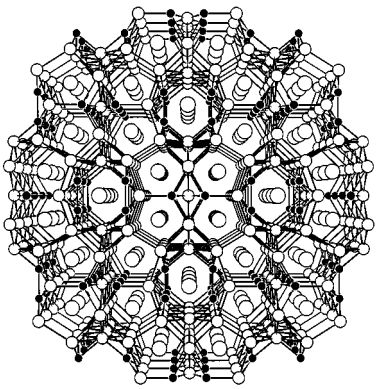

FIG. 4. Perspective view of the $Nd_5Ni_6In_{11}$ structure along the z direction. The complex three-dimensionally infinite $[Ni_6In_{11}]$ polyanion is outlined. The neodymium, nickel, and indium atoms are drawn as large open, small filled, and medium open circles, respectively. The viewing center corresponds to 1/2, 1/2, z of Fig. 2.

Ni–Ni distance of 244 pm, somewhat shorter than in elemental nickel (fcc (19), Ni–Ni = 249 pm). The coordination sphere of Ni1 with CN 9 is completed by five indium and three neodymium atoms. Ni2 has the closest contact to another Ni2 atom at 273 pm, significantly longer when compared with Ni1, avoiding the formation of Ni–Ni dumbbells. The Ni2 atoms additionally have five nearest indium and four neodymium neighbors, resulting in CN 10. The different nickel coordinations can easily be seen in the perspective view of the polyanion in Fig. 4.

The five crystallographically different indium positions all have CN 12 with nickel, indium, and neodymium atoms in their coordination spheres. The Ni–In distances range from 258 to 281 pm. The shorter ones compare well with the sum of the metallic single-bond radii of 265 pm for nickel and indium (20). The longest Ni–In distances are still shorter than the sum of the metallic radii for CN 12 of 291 pm (21). Similar short Ni–In distances are also observed in the $[NiIn_4]$ polyanion of $CeNiIn_4$ (6), with an average Ni–In distance of 267 pm. The diverse In–In distances cover the range from 298 to 321 pm. They all are shorter than in elemental indium (tetragonal distorted bcc variant), where each indium atom has four neighbors at 325 pm and additionally eight neighbors at 338 pm (19). The comparison of the interatomic distances clearly shows that the Ni–Ni pairs and the Ni–In and In–In bonding (most likely of covalent character) play an important role in the structure of $Nd_5Ni_6In_{11}$.

The structure of $Pr_5Ni_6In_{11}$ was originally discussed by Kalychak *et al.* (3) as an intergrowth of $CeMg_2Si_2$, Cu_3Au, CsCl, and $CeCo_3B_2$ slabs. This is only a more or less geometric description and it implies only little information on chemical bonding within this interesting class of compounds. We therefore favor the description of this unique crystal structure by the concept of polyanionic networks. The neodymium atoms are by far the most electropositive component of the compound and they will largely have transferred their valence electrons to the $[Ni_6In_{11}]$ network. To a first, very crude approximation, the formula of our compound may be written as $[5Nd^{3+}]^{15+}[Ni_6In_{11}]^{15-}$. A cutout of the complex three-dimensionally infinite $[Ni_6In_{11}]$ polyanion is presented in Fig. 4. Such complex

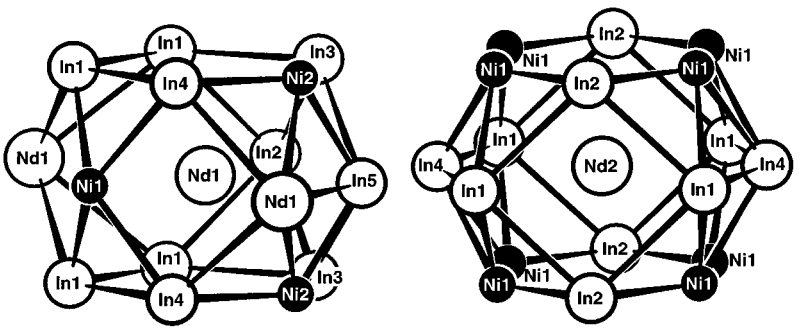

FIG. 3. Coordination polyhedra of the neodymium atoms in $Nd_5Ni_6In_{11}$.

polyanions with similar bonding characteristics also occur in structures such as $CeNiIn_4$ (6), Sc_2Ni_2In (7), Ti_2Ni_2In (11), or $NaAuIn_2$ (22). Although the description by a polyanionic network seems quite adequate at first, some words of caution seem to be appropriate, since some bonding interactions still remain between the neodymium and nickel (indium) atoms (see shortest distances in Table 3; Nd1–In5 = 321 pm, Nd1–Ni1 = 286 pm), indicating mixing of Nd and Ni (In)-centered bands at the Fermi level, in agreement with the metallic behavior discussed below.

Magnetic and Thermal Properties

The inverse molar magnetic susceptibility of a polycrystalline sample of $Nd_5Ni_6In_{11}$ measured in an external magnetic field of 0.01 T is displayed in the inset of Fig. 5. Above 150 K the inverse susceptibility follows a Curie–Weiss law with a paramagnetic Curie temperature of $-18(1)$ K, indicating predominantly antiferromagnetic interactions. The effective magnetic moment (per Nd atom) as extracted from the slope of the high-temperature inverse susceptibility is 3.60(5) μ_B, in very good agreement with the expected effective moment of 3.62 μ_B for Nd^{3+} with a $4f^3$ configuration and a $^4I_{9/2}$ ground-state term. At low temperatures (Fig. 5) the susceptibility exhibits three distinct features due to long-range magnetic ordering processes: At 11.4(1) K a maximum is observed which we attribute to the onset of long-range antiferromagnetic ordering. At around 6 K a broad shoulder appears and below 3 K a strong increase of the magnetic susceptibility is seen, presumably indicating ferrimagnetic ordering below this temperature. All these features indicate additional ordering processes or reorientations of the moments below the first ordering appearing at the Néel temperature of 11.4 K.

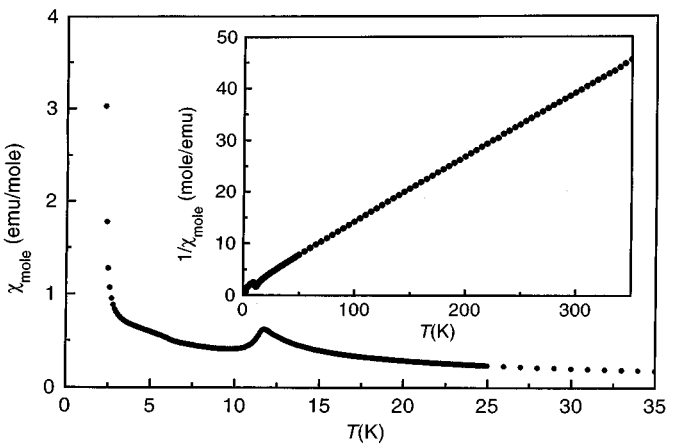

FIG. 5. Temperature dependence of the magnetic susceptibility of $Nd_5Ni_6In_{11}$ in an external field of 0.01 T below 35 K. The inset displays $1/\chi_{mol}$ at the same field for higher temperatures.

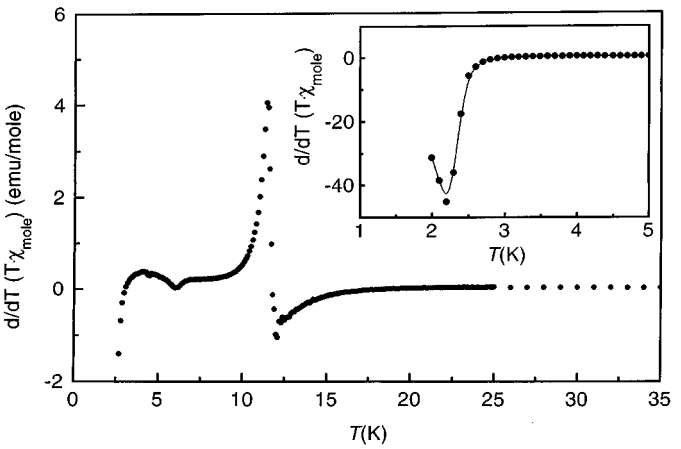

FIG. 6. Temperature derivative of $T\chi_{mol}$ plotted vs temperature. The inset shows the strong negative peak of $d/dT(T\chi_{mol})$ at low temperatures.

The anomalies associated with these ordering processes are clearly revealed in the temperature derivative of the quantity $T\chi_{mol}$ (Fig. 6). We note that there is a clear one-to-one correspondence of the anomalies in the specific heat (Fig. 7) and the quantity $d/dT(T\chi_{mol})$. In addition to the features already apparent in the direct susceptibility, a tiny anomaly at 4.4 K is resolved in the temperature derivative of $T\chi_{mol}$ which corresponds to the low-temperature shoulder of the strong 5 K peak in the specific heat. The susceptibility increase below 3 K shows up as a very large negative peak in the temperature derivative centered at 2.2 K (see inset of Fig. 6). The anomaly in heat capacity at 2.2 K as well supports the suggestion that the strong susceptibility increase below 3 K is a property of the bulk and does not originate from impurity phases. A magnetization measurement taken at 2 K displayed in Fig. 8 in fact proves a small ferromagnetic component which can be saturated already at a very moderate field of less than 0.05 T.

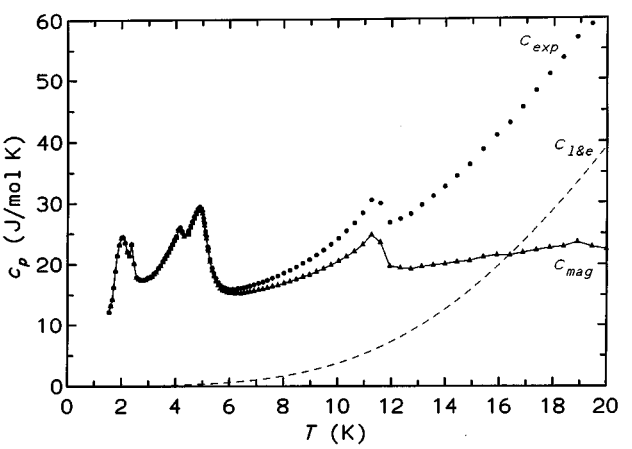

FIG. 7. Analysis of the specific heat capacity of $Nd_5Ni_6In_{11}$. c_{exp} (circles), experimental data; $c_{l\&e}$ (dashed line), lattice and electronic contributions; c_{mag} (triangles), magnetic 4*f* contributions (see text).

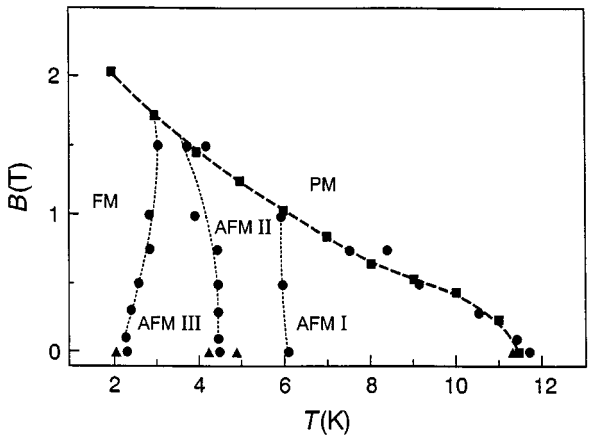

FIG. 8. Magnetic phase diagram of $Nd_5Ni_6In_{11}$. Data points are derived from susceptibility measurements with constant magnetic fields (circles), isothermal magnetization curves (squares), and specific heat data at zero field (triangles).

The specific heat up to 20 K is displayed in Fig. 7. For an estimate of the magnetic (4*f* electron) contribution $c_{mag}(T)$ to the specific heat, data of $La_5Ni_6In_{11}$ by Tang *et al.* (4) were utilized. The Debye temperature $\Theta_{D,La} = 266(18)$ K of $La_5Ni_6In_{11}$ for 1.5–3.0 K and values of $c_p(T)_{La}$ (4) converted to $\Theta_{D,La}(T)$ were scaled by the square root of the ratio of the molar masses (see, e.g., Ref. (23)) to obtain $\Theta_{D,Nd}(T)$ with $\Theta_{D,Nd}(0) = 264.5$ K. For the (non-*f* electron) Sommerfeld coefficient the value $\gamma = 4.5(4)$ mJ/mol K^2 (4) of the La compound was used. The background contribution ($c_{l\&e}$ = Debye curve + γT) and the derived magnetic contributions c_{mag} are given as lines in Fig. 7. As discussed for the curve of $d/dT(T\chi_{mol})$, distinct peaks at the magnetic transitions become visible. From the amplitudes, however, there is no congruence of both curves. The small specific heat peak at 11.5 K corresponds to a large peak in $d/dT(T\chi_{mol})$. Below the peak at 2.0 K the specific heat seems to finally attain a conventional T^{α} behavior with α in the range of 3. Above the Néel point a large, slightly increasing $c_{mag}(T)$ is visible, which we interpret as a multi-Schottky anomaly caused by crystal field effects of the neodymium atoms on the two crystallographically different sites. A splitting of the $^4I_{9/2}$ ground state into five doublets with different energy spacings for the two Nd sites is expected.

The entropy vs temperature behavior $S_{mag}(T)$ of the magnetic specific heat is complicated. $S_{mag} = 5R\ln 2$ is attained at 5.0 K, slightly above the spin-reordering peak at 4.9 K. Again slightly above the Néel temperature, $5R\ln 3$ is reached. However, the curve $S_{mag}(T)$ continues to rise smoothly due to low-lying crystal field levels. At 20 K the value $2 \times 5R\ln 2$ is reached; i.e., two doublets are thermally effectively excited. One may speculate on a partial ordering of the neodymium atoms, especially on the Nd1 and Nd2 sublattices. Nd1 (Wyckoff site 8*p*) has a four times larger multiplicity in the asymmetric unit when compared with Nd2 (Wyckoff site 2*c*). A clear distribution of magnetic entropy in this ratio is not obvious from the data, primarily due to the large magnetic background contribution under the modulation of $c_{mag}(T)$ by the phase transitions.

A tentative magnetic phase diagram of $Nd_5Ni_6In_{11}$ was gained from a set of temperature- and field-dependent magnetization measurements and the respective derivatives $d/dT(T\chi_{mol})$ at fixed field and $d/dB(M)$ at fixed temperatures (Fig. 8). The data points indicate the detected maxima in these quantities (Fig. 6). The phase diagram marks a sluggish transition from the paramagnetic to the ordered phases. The transition at zero field occurs at 11.5(2) K and at zero temperature the phase boundary extrapolates to 2.3(1) T. Four ordered phases can be identified, which have been labeled AFM I, AFM II, AFM III, and FM I, referring to the antiferromagnetic and ferri- or weak ferromagnetic phases, respectively. The occurrence of the FM I phase at low temperatures may have its origin in the presence of the two crystallographically different neodymium sites. They experience different electronic environments (i.e., electric field gradients) with different crystal field splitting and have therefore also different ground-state electronic wavefunctions. Even an antiparallel alignment of the two sublattices may then leave a small net moment which can be aligned in an external field.

The specific resistivity of $Nd_5Ni_6In_{11}$ (Fig. 9) decreases with decreasing temperature as is usually found for metallic conductors. The room temperature value of 120 μΩ cm is in the range generally observed for related indium intermetallics; e.g. $CeNiIn_4$ (6), $EuNiIn_4$ (9), and Sc_2Ni_2In (7) have room temperature specific resistivities of 33 μΩ cm, 14 μΩ cm, and 224 mΩ cm, respectively. Deviations from linearity above 50 K may be attributed to crystal field effects. The magnetic ordering is also seen in the specific resistivity as a slight drop at around 11 K (Fig. 9) due to freezing of spin-disorder scattering in the ordered state.

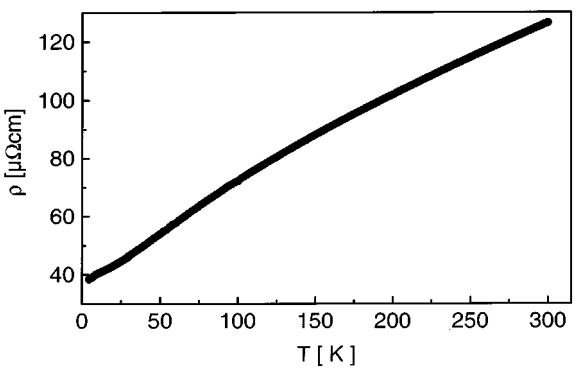

FIG. 9. Temperature dependence of the specific resistivity of $Nd_5Ni_6In_{11}$.

ACKNOWLEDGMENTS

The experimental part of this work was started in Stuttgart and finished in Münster. We thank Professor Arndt Simon and Professor Wolfgang Jeitschko for their interest and steady support of this work. We are also grateful to Eva Brücher for the susceptibility measurement and Nicola Rollbühler for the electrical conductivity measurement. This work was supported by the Deutsche Forschungsgemeinschaft (Po573/2-1) and the Fonds der Chemischen Industrie.

REFERENCES

1. P. Villars and L. D. Calvert, "Pearson's Handbook of Crystallographic Data for Intermetallic Phases," 2nd ed. ASM International, Materials Park, OH, 1991.
2. A. Szytuła and J. Leciejewicz, "Handbook of Crystal Structures and Magnetic Properties of Rare Earth Intermetallics." CRC Press, Boca Raton, FL, 1994.
3. Ya. M. Kalychak, P. Yu. Zavalii, V. M. Baranyak, O. V. Dmytrakh, and O. I. Bodak, *Sov. Phys. Crystallogr.* **32,** 600 (1987); *Kristallografiya* **32,** 1021 (1987).
4. J. Tang, K. A. Gschneidner, Jr., S. J. White, M. R. Roser, T. J. Goodwin, and L. R. Corruccini, *Phys. Rev. B* **52,** 7328 (1995).
5. R. Pöttgen, *Z. Naturforsch., B* **49,** 1525 (1994).
6. R. Pöttgen, *J. Mater. Chem.* **5,** 769 (1995).
7. R. Pöttgen and R. Dronskowski, *Z. Anorg. Allg. Chem.* **622,** 355 (1996).
8. R. Pöttgen, *J. Mater. Chem.* **6,** 769 (1996).
9. R. Pöttgen, R. Müllmann, B. D. Mosel, and H. Eckert, *J. Mater. Chem.* **6,** 801 (1996).
10. R. Pöttgen, *Z. Kristallogr.* **211,** 884 (1996).
11. R. Pöttgen and G. Kotzyba, *Z. Naturforsch., B* **51,** 1248 (1996).
12. R. Pöttgen and R. Dronskowski, *J. Solid State Chem.* **128,** 289 (1997).
13. Ya. M. Kalychak, *J. Less-Common Met.* **262–263,** 341 (1997).
14. H. L. Krauss and H. Stach, *Z. Anorg. Allg. Chem.* **366,** 34 (1969).
15. K. Yvon, W. Jeitschko, and E. Parthé, *J. Appl. Crystallogr.* **10,** 73 (1977).
16. E. Gmelin, *Thermochim. Acta* **110,** 183 (1987).
17. G. M. Sheldrick, SHELX-86, Program for the Solution of Crystal Structures, University of Göttingen, Göttingen, Germany, 1986.
18. G. M. Sheldrick, SHELXL-93, Program for Crystal Structure Refinement, University of Göttingen, Göttingen, Germany, 1993.
19. J. Donohue, "The Structures of the Elements." Wiley, New York, 1974.
20. L. Pauling, "The Nature of the Chemical Bond and the Structures of Molecules and Crystals." Cornell Univ. Press, Ithaca, NY, 1960.
21. E. Teatum, K. Gschneidner, Jr., and J. Waber, Report LA-2345, U.S. Department of Commerce, Washington, DC, 1960.
22. U. Zachwieja, *Z. Anorg. Allg. Chem.* **621,** 1677 (1995).
23. W. Schnelle, R. Pöttgen, R. K. Kremer, E. Gmelin, and O. Jepsen, *J. Phys.: Condens. Matter* **9,** 1435 (1997).